

Communication

Optimization of Anodization Parameters in Ti-30Ta Alloy

Patricia Capellato ^{1,*} , Daniela Sachs ¹, Lucas V. B. Vasconcelos ¹, Miriam M. Melo ², Gilbert Silva ², Maria G. A. Ranieri ³, Cecilia A. de C. Zavaglia ⁴, Roberto Z. Nakazato ⁵ , and Ana P. R. Alves Claro ⁶

¹ Institute of Physics and Chemistry, Unifei-Federal University of Itajubá, Av. BPS, 1303, Itajubá, 37500-903 Minas Gerais, Brazil; danisachs@unifei.edu.br (D.S.); vasconcelos.lvb@unifei.edu.br (L.V.B.V.)

² Institute of Mechanical Engineering, Unifei-Federal University of Itajubá, Av. BPS, 1303, Itajubá, 37500-903 Minas Gerais, Brazil; mirianmottamelo@unifei.edu.br (M.M.M.); gilbert@unifei.edu.br (G.S.)

³ Institute of Production Engineering and Management, Development, Technology and Society Program (DTEcS), Unifei-Federal University of Itajubá, Av. BPS, 1303, Itajubá, 37500-903 Minas Gerais, Brazil; gabirranieri@unifei.edu.br

⁴ Faculty of Mechanical Engineering, Unicamp-State University of Campinas, Rua Mendeleev, 200, Campinas, 13083-860 São Paulo, Brazil; zavagl@fem.unicamp.br

⁵ Department of Chemistry and Energy, School of Engineering, Unesp-São Paulo State University, Av. Ariberto Pereira da Cunha, 333, Guaratinguetá, 12516-410 São Paulo, Brazil; nakazato@feg.unesp.br

⁶ Materials and Technology Department, School of Engineering, Unesp-São Paulo State University, Av. Ariberto Pereira da Cunha, 333, Guaratinguetá, 12516-410 São Paulo, Brazil; Paula.rosifini@unesp.br

* Correspondence: capellato@unifei.edu.br; Tel.: +55-129-815-634-26

Received: 23 June 2020; Accepted: 31 July 2020; Published: 6 August 2020



Abstract: The current metallic biomaterial still presents failures associated with the bulk alloy and the interface of material/human body. In previous studies, titanium alloy with tantalum showed the elastic modulus decrease in comparison with that of commercially pure (cp) titanium. In this study, surface modification on Ti-30Ta alloy was investigated. Titanium and tantalum were melted, homogenized, cold-worked by a rotary swaging process and solubilized. The anodization process was performed in electrolyte contained glycerol + NH₄F 0.25% at 30 V using seven different durations—4 h, 5 h, 6 h, 7 h, 8 h, 9 h, and 10 h and annealed at 530 °C for 1 h. The surface topography was characterized by scanning electron microscopy (SEM), atomic force microscopy (AFM) measurements, X-ray diffraction analysis (XRD), and contact angle. From the results, we conclude the time of anodization process influences the shape and morphology of the anodized layer. The 5 h-anodization process produced a smooth and porous surface. The 4-, 6-, 7-, 8-, 9-, and 10-h conditions showed nanotubes morphology. All surfaces are hydrophilic (<90°). Likewise, all the investigated conditions present anatase phase. So, this surface modification presents potential for biomedical application. However, more work needs to be done to better understand the influence of time on the anodization process.

Keywords: TiO₂ nanotube; Ti-30Ta alloy; anodization process; anatase phase; nanostructured material

1. Introduction

Metallic medical devices have been used to replace parts of the body due to suitable mechanical properties and biocompatibility. Despite, the current material in use, including stainless steels, Co-Cr based alloys, titanium, and its alloys still present failures associated with the bulk of the alloy and the interface of material/human body. Recently, the cost of correction of those failures is high and it inspires studies for a new solution [1–5].

Human bone tissue has mechanical properties such as high resistance to fatigue, low modulus of elasticity, and resistance to wear and corrosion. So, the ideal biomaterial must have mechanical properties comparable to the natural tissue where it is inserted so that there is no additional tension to the surrounding tissue [6,7]

Research has been carried out with titanium [1,8] and its alloys in order to achieve the ideal biomaterial for biomedical application. However, the titanium low mechanical strength and the cytotoxic effects attributed to the use of Ti-6Al-4V alloy, such as Alzheimer's disease [9,10] has led to the development of metals with non-toxic elements addition for example, Ta, Zr, Nb, Hf, Mo, and Sn [11–13].

Mechanical properties such as elastic modulus cause a phenomenon called stress shielding that has been pointed out as being the highest reason for implant failure. Stress shielding phenomenon results bone density reduction due different deforming resistance and constant bone-implant friction. Researchers have searched an alloy that presents an elastic modulus near to the bone, around 10–30 GPa, in order to avoid stress shielding [14,15].

Recent research has investigated the Ti-Ta binary system to find the ideal proportion of added tantalum to obtain better mechanical and biocompatibility properties. Metallic implant alloys such stainless steel ($E = 200$ GPa), cobalt alloy ($E = 275$ – 1585 GPa), CP titanium ($E = 105$ GPa), and Ti-6Al-4V ($E = 110$ GPa) show elastic modulus higher than bone ($E = 10$ – 30 GPa). Among the tested alloys, Ti with 30% Ta ($E = 69$ GPa) shows elastic modulus closer to bone [14–18].

Likewise, previous studies have shown the important role of the surface on the interaction implant/host spot cell interaction. Then, surface coating with nanostructure topography presents desirable cell response for biomaterial purpose [19–26].

However, no prior studies have evaluated the influence of different nanotubes fabrication parameters on these promising Ti-30Ta alloys. Thus, we investigate the formation of nanotubular structure on the surface of Ti-30Ta alloy, controlling the parameters of anodization. Then, in this study, we investigated seven different anodization time processes. In this way, nanotubular surface was obtained with different diameters and lengths that could lead to different cellular responses.

2. Materials and Methods

2.1. Process of Ti-30Ta Alloy

The Ti-30Ta wt.% alloy was processed according to our previous studies [19]. Briefly, titanium and tantalum pure (99.99%) (Sorocaba, Brasil) were melt in a high purity argon atmosphere mixing, both purchased from Sigma-Aldrich. The obtained ingot was homogenized in a vacuum at 1000 °C for 24 h. The alloy was then cold-worked by a rotary swaging process and solubilized at 950 °C for 2 h followed by water-cooling. The bars were cut into discs of 6 mm in diameter and 3 mm in thickness [22,23].

2.2. Surface Treatment

The anodization process was described on previous studies [27]. Summarily, dual electrode system with platinum (counter electrode) and Ti-30Ta alloy (working electrode) fixed 15 mm apart for anodization process. The electrodes were then suspended in an electrolyte contained glycerol and NH_4F 0.25%. The electrodes were connected to a power supply (Fisher Scientific FB300 Electrophoresis) and the voltage applied was 30 V at room temperature. They were investigated at seven different durations: 4, 5, 6, 7, 8, 9, and 10 h. Following the anodization process, the Ti-30Ta alloy substrate was rinsed in isopropyl alcohol and dried by compressed air. All anodized substrates were further annealed in an oxygen ambient furnace at 530 °C, with a ramping rate of 5 °C/min for 1 h [27]. Each experiment was reconfirmed on at least three different substrates.

2.3. Characterization of Substrates

The surface topography of seven different durations: 4, 5, 6, 7, 8, 9, and 10 h was characterized by scanning electron microscopy (SEM) imaging (JEOL JSM 6100) (Carl Zeiss, Guaratingueta, Brazil) with 10 mm working distance and 15 keV. Prior to imaging, all substrates were coated with a 15 nm layer of gold. In order to obtain cross-sectional images, the surface was mechanically scratched with metallic tool and imaged by tilting the chamber to 70° and changing the working distance to 4.6 mm. Atomic force microscopy (AFM) (Shimadzu, Guaratinguetá, Brazil) measurements were performed using a Dimension Icon microscope (Shimadzu, Guaratinguetá, Brazil) from Shimadzu, operating in non-contact mode. The root mean square (RMS) roughness was measured in a $2 \times 2 \mu\text{m}^2$ area. The wettability of the substrate surfaces was investigated using a sessile drop method (2 mL) with a contact angle goniometer (Kruss DSA 10) (Kruss, Guaratinguetá, Brazil), equipped with video capture. The contact angle was measured through the liquid, where a liquid-vapor interface meets a solid surface. The resulting images at the water-substrate interface were fit using the circle fitting profile [28]. The crystallinity of the substrates was investigated by X-ray diffraction analysis (XRD), using a X'Pert Philips PMD (Philips, São Carlos, Brazil) with a Panalytical X'celerator detector using a Monochromatic $\text{CuK}\alpha$ radiation (Philips, São Carlos, Brazil) ($\lambda = 0.1544 \text{ nm}$) applied at 20 mA and 40 kV, with a step size of 0.02° , and a collecting time of 1.6 s.

3. Results and Discussion

The nano topography has high influence on the success of metallic implantable device [11,26,28–31]. Thus, we investigate the formation of nanotubular structure on the surface of Ti-30Ta alloy controlling the parameters of anodization. The anodizing process is an electrochemical reaction. The name “anodize” comes from the fact that the substrate will be the anode. The substrate is immersed in an electrolyte solution with another material that will be the cathode. The current passes through the acidic solution, hydrogen from the cathode is released and oxygen from the anode surface is released as well. The reaction of these elements forms a film on the surface of the substrate.

The anodization process was performed in an electrolyte solution containing NH_4F 0.25% + glycerol [32] and applied voltage at 30 V to at least three substrates with good repeatability. Seven different conditions on variation of time were investigated (Figures 1 and 2). In this way, nanotubular surface was obtained with different diameters and lengths that could lead to different cellular responses [20,27,33–36].

SEM images (Figures 1 and 2) show the Ti-30Ta alloy surface after anodization process for 4, 5, or 6 h. The annealing process was performed at 530°C for 1 h.

In Figure 1a-c SEM micrographs of the surface of the Ti-30Ta alloy after anodization process for 4, 5, and 6 h at different magnifications were depicted. Figure 1(4h-a,6h-c) present a precursor geometric formation of pores/nanotube with nonhomogeneous morphology and cracks. According to Zhou (2005) TiO_2 oxides are observed on the surface of titanium and its alloys, but it was not found by the authors for Ti-30Ta alloy, with the passive layer of Ta_2O_5 being more stable [16]. A circular formation for the 5- and 6-h conditions and nanotubes in 4 h can be observed in higher magnification.

Also, the surface of 5-h anodization (Figure 1(5h-b)) presents smooth surface. Therefore, the presence of pores and nanotubes is confirmed for the 4-and 6-h conditions, which does not occur with the 5-h anodization (Figure 1(5h-a-c)). The 5-h anodization does not allow the formation of nanotubes.

Increasing the anodization time at the same voltage and electrolyte leads to nanotubular formation with similar morphologies and lengths [37]. Figure 2a-c shows micrographs in different magnifications of the surface of the Ti-30Ta alloy submitted to anodization process at 30 V for 7, 8, 9, and 10 h. When the anodic time was increased, nanotubes were coated with a homogeneous and regular layer (Figure 2a-c). Nanotubes with an oval shape and significant length were obtained for the four conditions (Figure 2b,c). When increasing anodization time, the entire surface of the alloy is covered with nanotubes in a homogeneous and regular manner (Figure 2b). For the 9-h anodization (Figure 2(9h-c)) the diameter of

nanotube is slightly larger than 7, 8, and 10 h. Tsuchiya et al., in 2009, investigated Ti-xTa ($x = 13, 25, 50,$ and 80 wt.%) anodization process and electrolyte $\text{H}_2\text{SO}_4 + \text{HF} + \text{H}_2\text{O}$ at 20 V for 3 h [28] and other authors shows similar results [38].

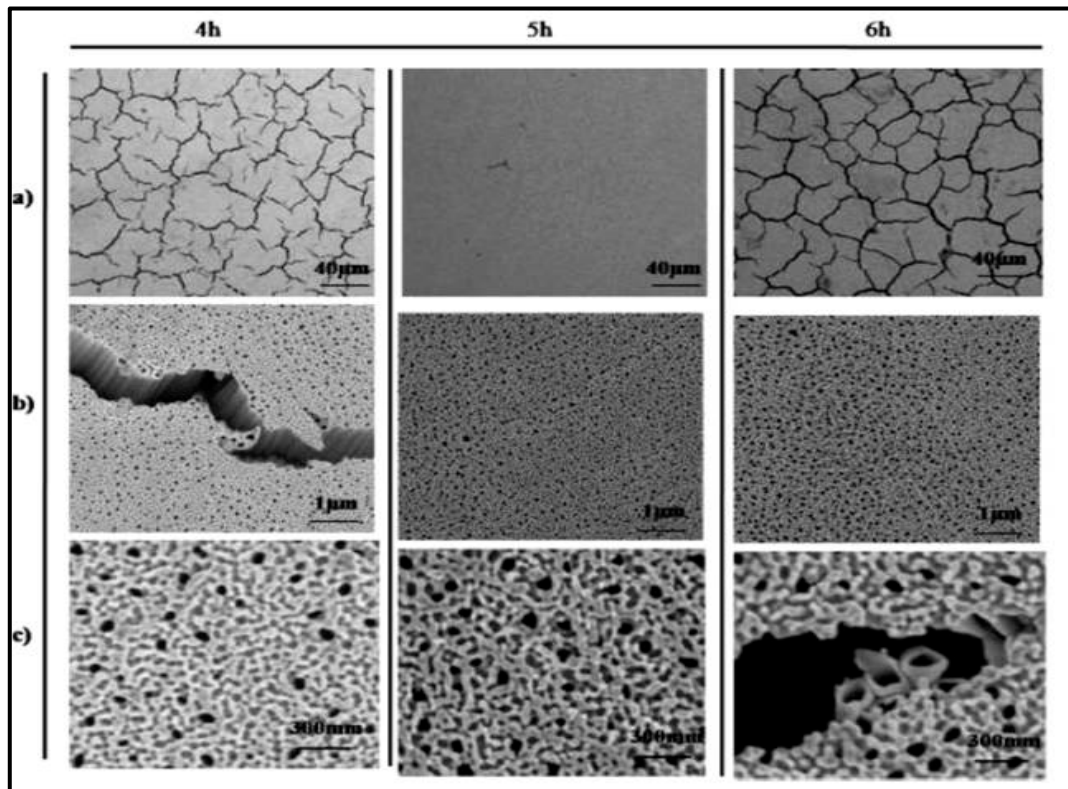


Figure 1. Scanning electron microscopy (SEM) images of Ti-30Ta alloy surface after anodization process in NH_4F 0.25% + glycerol at 30 V for $4, 5,$ and 6 h. The annealing process was performed at 530 °C (5 °C/min) for 1 h. (a) Micrographs of superficial morphology. (b) Micrographs of superficial morphology in higher magnification. Nanotubes cover the substract surface. (c) Tilted micrographs of superficial morphology. They show the morphology height.

The software ImageJ was used to determine the diameter and length of the nanotubes formed on the surface of the Ti-30Ta alloy after anodizing at 30 V for $4, 5, 6, 7, 8, 9,$ and 10 h.

Table 1 shows the formed nanotube diameter and length. The nanotube diameter can be described from the smallest to the largest diameter as follows: 4 h— 26.41 ± 0.94 nm, 6 h— 28.79 ± 1.17 nm, 7 h— 32.67 ± 2.51 nm, 8 h— 42.77 ± 1.87 nm, 10 h— 42.32 ± 2.31 nm, and 9 h— 57.21 ± 3.27 nm. For the nanotube length values, the order of lowest to highest increase differs from that followed by the standard diameter being: 4 h— 7.13 ± 1.57 μm , 6 h— 6.88 ± 1.73 μm , 9 h— 6.54 ± 2.09 μm , 7 h— 6.87 ± 1.68 μm , 8 h— 7.25 ± 0.97 μm , and 10 h— 8.61 ± 1.36 μm . According to the literature, the increase in layer thickness is related to the anodizing time [39–42]. With the increase of the oxide layer thickness, it was possible to dissolve and form the compact oxide layer and the formation of nanotubes. The nanotube can mimic the shape of alveolar bone (Table 1).

The ideal condition was obtained within 9 h (Figure 2(9h-b)). These results show nanotubes in the dimensions of 57.21 ± 3.27 nm in diameter and 6.54 ± 2.09 μm in length. Studies with pure titanium show that similar dimensions provide an increase in functionality [38,43–45] and hemocompatibility [33,36].

X-ray diffraction analysis were applied to assess the phase changes that occurred during all conditions of the anodizing process. Figure 3 shows the obtained spectra after anodizing process. All investigated conditions showed anatase phase with the greatest peaked around 25° , the exception

is the control group. The anatase phase provides an improvement in the cellular response required in biomedical applications [33,46–48].

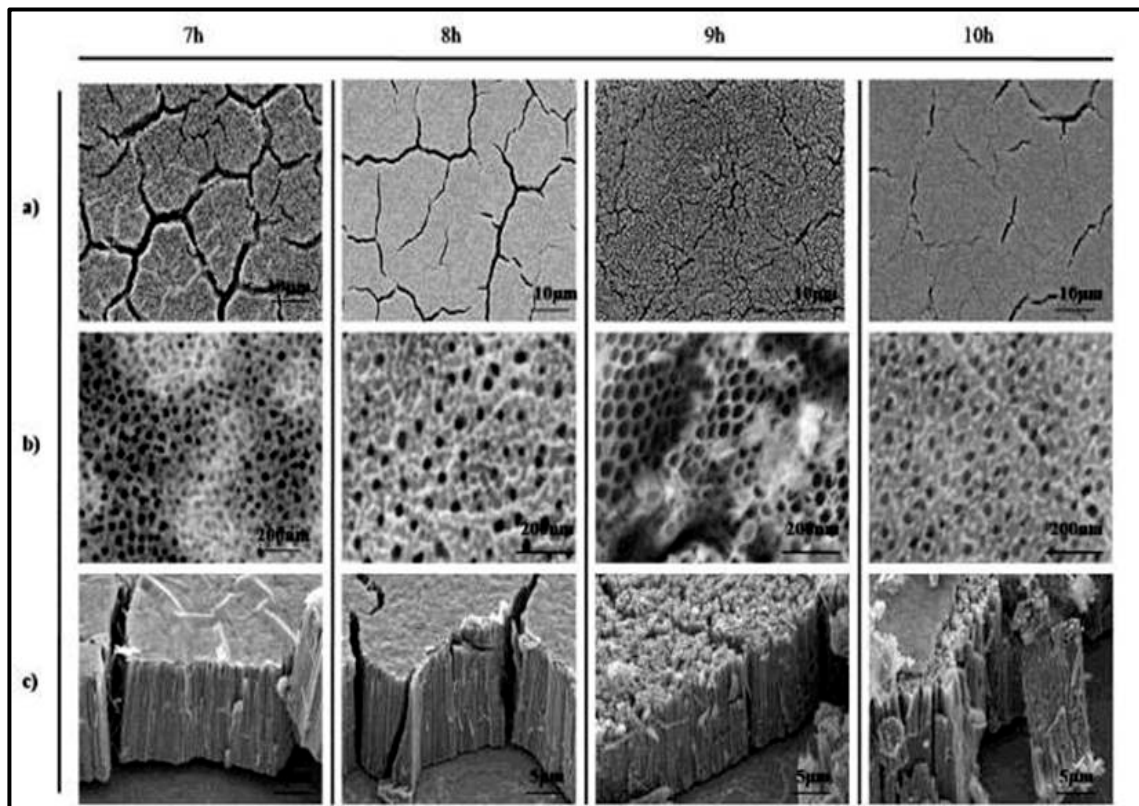


Figure 2. SEM images of Ti-30Ta alloy surface after anodization process in NH_4F , 25% + glycerol at 30 V for 7, 8, 9, and 10 h. The annealing process was performed at 530 °C (5 °C/min) for 1 h. (a) Micrographs of superficial morphology. (b) Micrographs of superficial morphology in higher magnification. Nanotubes cover the substract surface. (c) Tilted micrographs of superficial morphology. They show the morphology height.

Table 1. Diameter and length measurements of the nanotubes formed on the surface of the Ti-30Ta alloy a SEM images of Ti-30Ta alloy surface after anodization process in NH_4F 0.25% + glycerol at 30 V for 4, 5, 6, 7, 8, 9, and 10 h. The annealing process was performed at 530 °C (5 °C/min) for 1 h.

Anodization Time (h)	Nanotube Diameter (nm)	Nanotube Length (μm)
4	26.41 ± 0.94	7.13 ± 1.57
5	00.00	00.00
6	28.79 ± 1.17	6.88 ± 1.73
7	32.67 ± 2.51	6.87 ± 1.68
8	42.77 ± 1.89	7.25 ± 0.97
9	57.21 ± 3.24	6.54 ± 2.09
10	42.32 ± 2.31	8.61 ± 1.36

We can observe in Figures 4 and 5, the surface topography obtained by atomic force microscopy (AFM). The data was processed with the Shimadzu SPM software (Scanning Probe Microscopy) offline V.3.31 (Guaratinguetá, Brazil). The substrates subjected to anodizing for 4, 5 and 6 h (Figure 4) presented a surface with irregular topography and some differences in the topography occurred for 7, 8, 9, and 10 h (Figure 5) which can be attributed to the formation of nanotubes on the substrate surface after the anodizing process. The condition of 10 h shows a greater change in the surface topography.

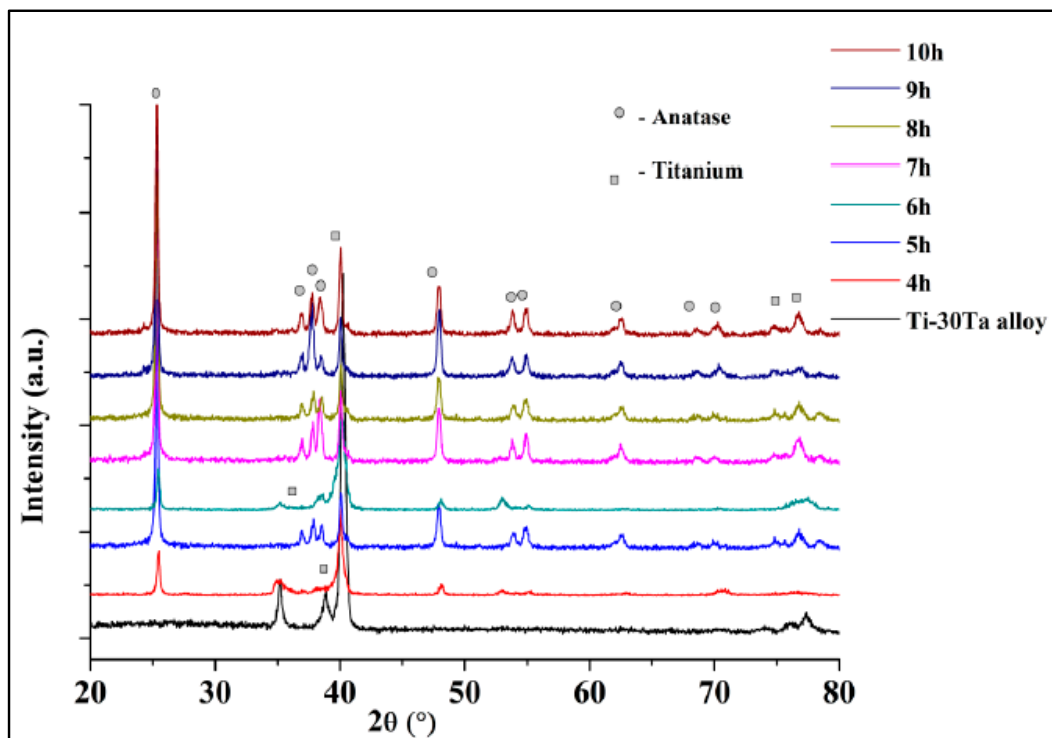


Figure 3. X-ray diffraction analysis (XRD) patterns of Ti-30Ta alloy and after anodization process in NH_4F 0.25% + glycerol at 30 V for 4, 5, 6, 7, 8, 9, and 10 h. The annealing process was performed at $530\text{ }^\circ\text{C}$ ($5\text{ }^\circ\text{C}/\text{min}$) for 1 h. We observed anatase formation for all conditions except the control group.

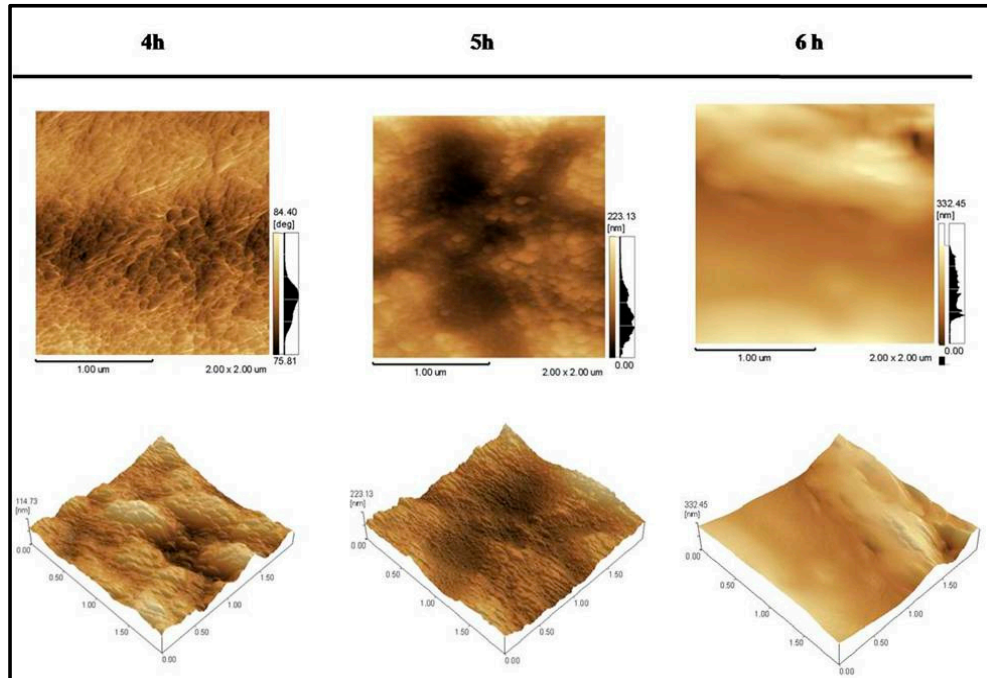


Figure 4. Images obtained in an atomic force electron microscope (AFM) after anodization process in NH_4F 0.25% + glycerol at 30 V for 4, 5, and 6 h. The annealing process was performed at $530\text{ }^\circ\text{C}$ ($5\text{ }^\circ\text{C}/\text{min}$) for 1 h.

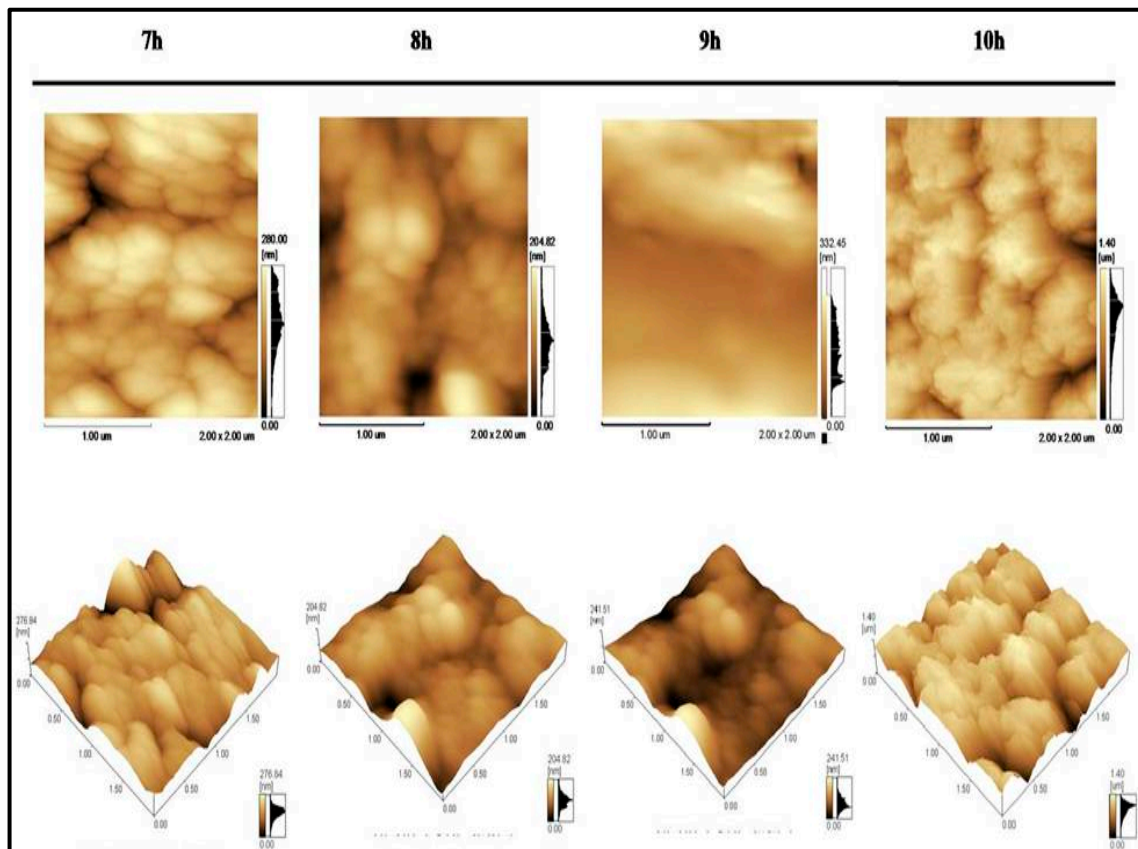


Figure 5. Images obtained in an atomic force electron microscope (AFM) after anodization process in NH_4F 0.25% + glycerol at 30 V for 7, 8, 9, and 10 h. The annealing process was performed at 530 °C (5 °C/min) for 1 h.

The human tissue features variations in which they promote specific protein adsorption and direct chemical interactions through the cellular behavior. Thus, these nanotube topographic characteristics (Figures 4 and 5) allow a promising interface due to an increase in the nanometric scale roughness of the material surface [49].

The values of mean roughness (R_a) were obtained analyzing substrates in AFM. The values follows: 4 h— 121.28 ± 2.47 nm, 5 h— 124.56 ± 0.76 nm, 6 h— 121.19 ± 1.59 nm, 7 h— 179.26 ± 1.42 nm, 8 h— 127.35 ± 2.09 nm, 9 h— 124.34 ± 2.54 nm, and 10 h— 96.49 ± 1.98 nm (Figure 6). The proximity of the observed values in the anodized substrate for 4, 5, 6, 8, and 9 h. The 7-h anodization presented the highest roughness and 10 h, the lowest one. The roughness values influence the strength of cellular adhesion on the surface of the implanted biomaterial [34].

In addition, the wettability of the biomaterial can influence the cell response along with the topographic and roughness surface characteristics. In biomedical applications, wettability is a desirable condition since it promotes increase in cellular interaction [28,50]. Previous studies already related to the surface energy of a biomaterial with cellular functionality, such as protein adsorption, platelet adhesion and activation that leads to blood clotting and bacterial adhesion [51–54].

According to contact angle results, almost all surfaces are hydrophilic ($<90^\circ$). The values can be represented by the smallest angle to the largest as follows: 10 h ($36.66^\circ \pm 1.39^\circ$), 6 h ($38.83^\circ \pm 2.27^\circ$), 7 h ($38.90^\circ \pm 2.05^\circ$), 9 h ($39.46^\circ \pm 2.52^\circ$), 5 h ($39.99^\circ \pm 1.99^\circ$), 4 h ($40.99^\circ \pm 3.18^\circ$), and 8 h ($41.31^\circ \pm 0.96^\circ$). The conditions of 4, 5, and 7 h have close values, such as 10, 6, and 9 h.

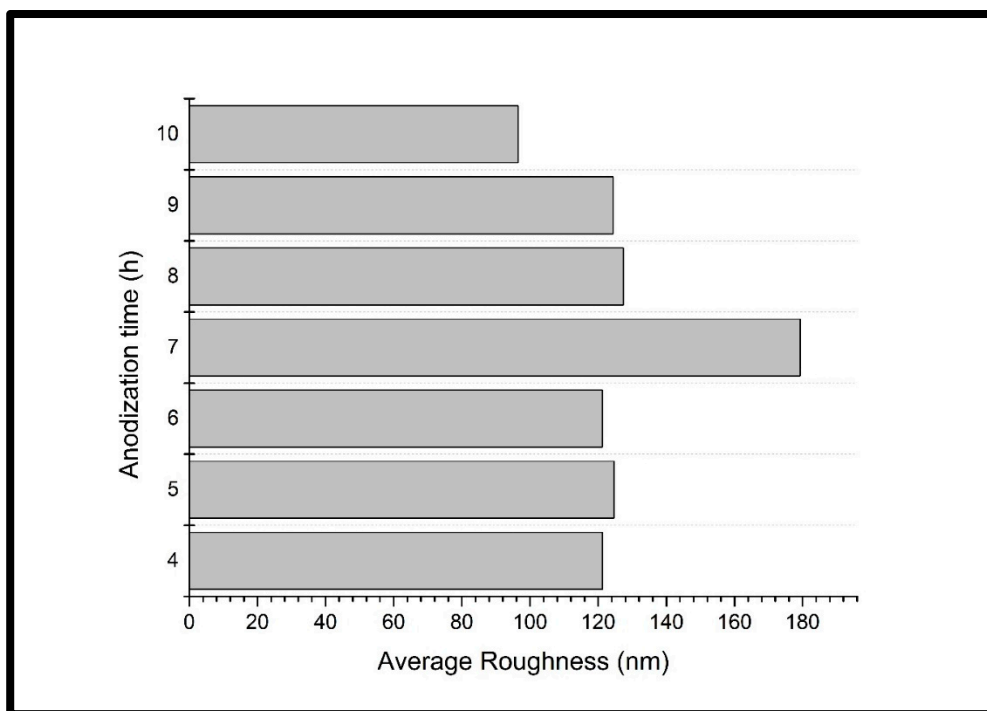


Figure 6. Values of mean roughness (Ra) after anodization process in NH_4F 0.25% + glycerol at 30 V for 4, 5, 6, 7, 8, 9, and 10 h. The annealing process was performed at 530 °C (5 °C/min) for 1 h.

4. Conclusions

The search for an ideal metallic biomaterial has been a challenge. Implantable devices for orthopedic and dental application must present elastic modulus near to the bone ($E = 10 - 30$ GPa) and nanoscale surface topographies to improve the interface response between material/human body. This study investigated the formation of nanotubular structure on the surface of Ti-30Ta alloy with elastic modulus ($E = 69$ GPa). From the results obtained so far, it was concluded that time variation of anodization process influences on growth of pore and nanotube structure. The 5-h anodization process produced a smooth surface. However, the presence of pores and nanotubes is confirmed by the 4-, 6-, 7-, 8-, 9-, and 10-h anodization process. According to the contact angle results, all surfaces are hydrophilic ($<90^\circ$). All the investigated conditions showed anatase phase with greatest peaked around 25° . So, this surface modification presents potential for biomedical application. Therefore, more work needs to be done to understand the anodization process.

Author Contributions: Conceptualization, A.P.R.A.C.; methodology, A.P.R.A.C., P.C. and R.Z.N.; software, P.C.; validation, P.C.; formal analysis, P.C.; investigation, P.C.; resources, C.A.d.C.Z., G.S., M.M.M. and D.S.; data curation, P.C.; writing—original draft preparation, P.C.; writing—review and editing, L.V.B.V., M.G.A.R. and P.C.; visualization, A.P.R.A.C.; supervision, A.P.R.A.C., C.A.d.C.Z.; project administration, A.P.R.A.C.; funding acquisition, C.A.d.C.Z., G.S., M.M.M., D.S. and A.P.R.A.C. All authors have read and agreed to the published version of the manuscript.

Funding: This research was funded by Brazilian federal government and the National Council for Scientific, Technological Development (CNPq) and Capes, grant number 201271/2010-9 and 486352/2013-7. Also, São Paulo Research Foundation (Fapesp), grant number 2014/14533-3. The APC was funded by Federal University of Itajubá (Unifei).

Conflicts of Interest: The authors declare no conflict of interest.

References

1. Verma, R.P. Materials Today: Proceedings Titanium based biomaterial for bone implants: A mini review. *Mater. Today Proc.* **2020**, *26*, 3148–3151. [CrossRef]
2. Biswal, T.; BadJena, S.K.; Pradhan, D. Sustainable biomaterials and their applications: A short review. *Mater. Today Proc.* **2020**. Available online: <https://www.sciencedirect.com/science/article/pii/S2214785320305423> (accessed on 24 January 2020). [CrossRef]
3. Chouirfa, H.; Bouloussa, H.; Migonney, V.; Falentin-Daudré, C. Review of titanium surface modification techniques and coatings for antibacterial applications. *Acta Biomater.* **2019**, *83*, 37–54. [CrossRef]
4. Pandey, A.; Awasthi, A.; Saxena, K.K. Metallic implants with properties and latest production techniques: A review. *Adv. Mater. Process. Technol.* **2020**, *6*, 405–440. [CrossRef]
5. Delanois, R.E.; Mistry, J.B.; Gwam, C.U.; Mohamed, N.S.; Choksi, U.S.; Mont, M.A. Current Epidemiology of Revision Total Knee Arthroplasty in the United States. *J. Arthroplasty* **2017**, *32*, 2663–2668. [CrossRef] [PubMed]
6. Niinomi, M. Recent Progress in Research and Development of Metallic Structural Biomaterials with Mainly Focusing on Mechanical Biocompatibility. *Mater. Trans.* **2018**, *59*, 1–13. [CrossRef]
7. Kurella, A.; Dahotre, N.B. Review paper: Surface modification for bioimplants: The role of laser surface engineering. *J. Biomater. Appl.* **2005**, *20*, 5–50. [CrossRef] [PubMed]
8. Grimes, C.A.; Varghese, O.K.; Feng, X.; Mor, G.K.; LaTempa, T.J.; Basham, J.I. Ta₃N₅ Nanotube Arrays for Visible Light Water Photoelectrolysis. *Nano Lett.* **2010**, *10*, 948–952. [CrossRef]
9. Walker, P.R.; LeBlanc, J.; Sikorska, M. Effects of aluminum and other cations on the structure of brain and liver chromatin. *Biochemistry* **1989**, *28*, 3911–3915. [CrossRef]
10. Zaffe, D.; Bertoldi, C.; Consolo, U. Accumulation of aluminium in lamellar bone after implantation of titanium plates, Ti-6Al-4V screws, hydroxyapatite granules. *Biomaterials* **2004**, *25*, 3837–3844. [CrossRef]
11. Besinis, A.; Hadi, S.D.; Le, H.R.; Tredwin, C.; Handy, R.D. Antibacterial activity and biofilm inhibition by surface modified titanium alloy medical implants following application of silver, titanium dioxide and hydroxyapatite nanocoatings. *Nanotoxicology* **2017**, *11*, 327–338. [CrossRef] [PubMed]
12. Wilson, J. Metallic biomaterials: State of the art and new challenges. *Fundam. Biomater. Met.* **2018**, 1–33. [CrossRef]
13. Chen, Q.; Thouas, G.A. Metallic implant biomaterials. *Mater. Sci. Eng. R Rep.* **2015**, *87*, 1–57. [CrossRef]
14. Zhou, Y.L.; Niinomi, M. Ti-25Ta alloy with the best mechanical compatibility in Ti-Ta alloys for biomedical applications. *Mater. Sci. Eng. C* **2009**, *29*, 1061–1065. [CrossRef]
15. Zhou, Y.L.; Niinomi, M.; Akahori, T. Effects of Ta content on Young's modulus and tensile properties of binary Ti-Ta alloys for biomedical applications. *Mater. Sci. Eng. A* **2004**, *371*, 283–290. [CrossRef]
16. Zhou, Y.L.; Niinomi, M.; Akahori, T.; Fukui, H.; Toda, H. Corrosion resistance and biocompatibility of Ti-Ta alloys for biomedical applications. *Mater. Sci. Eng. A* **2005**, *398*, 28–36. [CrossRef]
17. Zhou, Y.L.; Niinomi, M.; Akahori, T. Decomposition of martensite α'' during aging treatments and resulting mechanical properties of Ti-Ta alloys. *Mater. Sci. Eng. A* **2004**, *384*, 92–101. [CrossRef]
18. Zhou, Y.L.; Niinomi, M. Microstructures and mechanical properties of Ti-50 mass% Ta alloy for biomedical applications. *J. Alloys Compd.* **2008**, *466*, 535–542. [CrossRef]
19. Capellato, P.; Escada, A.L.A.; Popat, K.C.; Claro, A.P.R.A. Interaction between mesenchymal stem cells and Ti-30Ta alloy after surface treatment. *J. Biomed. Mater. Res. Part A* **2014**, *102*. [CrossRef]
20. Capellato, P.; Smith, B.S.; Popat, K.C.; Alves Claro, A.P.R. Cellular functionality on nanotubes of Ti-30Ta alloy. In *Materials Science Forum*; Trans Tech Publications Ltd.: Foz de Iguaçu, Brazil, 2015; Volume 805, ISBN 9783038352365.
21. Wong, J.Y.; Leach, J.B.; Brown, X.Q. Brown. Balance of chemistry, topography, and mechanics at the cell—Biomaterial interface: Issues and challenges for assessing the role of substrate mechanics on cell response. *Surf. Sci.* **2004**, *570*, 119–133. [CrossRef]
22. Capellato, P.; Riedel, N.A.; Williams, J.D.; Machado, J.P.B.; Popat, K.C.; Claro, A.P.R.A. Surface Modification on Ti-30Ta Alloy for Biomedical Application. *Engineering* **2013**, *5*, 707–713. [CrossRef]
23. Capellato, P.; Riedel, N.A.; Williams, J.D.; Machado, J.P.B.; Ketul Popat, K.C.; Alves Claro, A.P.R. Ion Beam Etching on Ti-30Ta Alloy for Biomedical Application. In *Materials Science Forum*; Trans Tech Publications Ltd.: Foz de Iguaçu, Brazil, 2015; Volume 805, ISBN 9783038352365.

24. Oh, S.; Daraio, C.; Chen, L.H.; Pisanic, T.R.; Fiñones, R.R.; Jin, S. Significantly accelerated osteoblast cell growth on aligned TiO₂ nanotubes. *J. Biomed. Mater. Res. Part A* **2006**, *78*, 97–103. [[CrossRef](#)] [[PubMed](#)]
25. Simi, V.S.; Rajendran, N. Influence of tunable diameter on the electrochemical behavior and antibacterial activity of titania nanotube arrays for biomedical applications. *Mater. Charact.* **2017**, *129*, 67–79. [[CrossRef](#)]
26. Regonini, D.; Bowen, C.R.; Jaroenworarluck, A.; Stevens, R. A review of growth mechanism, structure and crystallinity of anodized TiO₂ nanotubes. *Mater. Sci. Eng. R Rep.* **2013**, *74*, 377–406. [[CrossRef](#)]
27. Capellato, P.; Smith, B.S.; Popat, K.C.; Claro, A.P.R.A. Fibroblast functionality on novel Ti30Ta nanotube array. *Mater. Sci. Eng. C* **2012**, *32*, 2060–2067. [[CrossRef](#)]
28. Kim, I.-H.; Kwon, T.-Y.; Kim, K.-H. Wetting Behavior of Dental Implants. *Wetting Wettability* **2015**. [[CrossRef](#)]
29. Liu, Y.; Rath, B.; Tingart, M.; Eschweiler, J. Role of implants surface modification in osseointegration: A systematic review. *J. Biomed. Mater. Res. Part A* **2020**, *108*, 470–484. [[CrossRef](#)] [[PubMed](#)]
30. Marien, C.B.D.; Cottineau, T.; Robert, D.; Drogui, P. TiO₂ Nanotube arrays: Influence of tube length on the photocatalytic degradation of Paraquat. *Appl. Catal. B Environ.* **2016**, *194*, 1–6. [[CrossRef](#)]
31. Aguirre Ocampo, R.; Echeverría Echeverría, F. Effect of the anodization parameters on TiO₂ nanotubes characteristics produced in aqueous electrolytes with CMC. *Appl. Surf. Sci.* **2019**, *469*, 994–1006. [[CrossRef](#)]
32. Tsuchiya, H.; Schmuki, P. Less known facts and findings about TiO₂ nanotubes. *Nanoscale* **2020**, *12*, 8119–8132. [[CrossRef](#)]
33. Smith, B.S.; Yoriya, S.; Grissom, L.; Grimes, C.A.; Popat, K.C. Hemocompatibility of titania nanotube arrays. *J. Biomed. Mater. Res. Part A* **2010**, *95*, 350–360. [[CrossRef](#)] [[PubMed](#)]
34. Smith, B.S.; Capellato, P.; Kelley, S.; Gonzalez-Juarrero, M.; Popat, K.C. Reduced in vitro immune response on titania nanotube arrays compared to titanium surface. *Biomater. Sci.* **2013**, *1*. [[CrossRef](#)] [[PubMed](#)]
35. Smith, B.S.; Yoriya, S.; Johnson, T.; Popat, K.C. Dermal fibroblast and epidermal keratinocyte functionality on titania nanotube arrays. *Acta Biomater.* **2011**, *7*, 2686–2696. [[CrossRef](#)]
36. Hu, N.; Wu, Y.; Xie, L.; Yusuf, S.M.; Gao, N.; Starink, M.J.; Tong, L.; Chu, P.K.; Wang, H. Enhanced interfacial adhesion and osseointegration of anodic TiO₂ nanotube arrays on ultra-fine-grained titanium and underlying mechanisms. *Acta Biomater.* **2020**, *106*, 360–375. [[CrossRef](#)] [[PubMed](#)]
37. Qadir, M.; Lin, J.; Biesiekierski, A.; Li, Y.; Wen, C. Effect of Anodized TiO₂-Nb₂O₅-ZrO₂ Nanotubes with Different Nanoscale Dimensions on the Biocompatibility of a Ti35Zr28Nb Alloy. *ACS Appl. Mater. Interfaces* **2020**, *12*, 6776–6787. [[CrossRef](#)] [[PubMed](#)]
38. Sankara Narayanan, T.S.N.; Kim, J.; Park, H.W. Fabrication and synthesis of uniform TiO₂ nanoporous and nanotubular structures on dual-phase Ti–6Al–4V alloy using electron-beam irradiation. *Mater. Chem. Phys.* **2020**, *242*, 122549. [[CrossRef](#)]
39. El-Sayed, H.A.; Birss, V.I. Controlled growth and monitoring of tantalum oxide nanostructures. *Nanoscale* **2010**, *2*, 793–798. [[CrossRef](#)]
40. El-sayed, H.A.; Birss, V.I. Controlled formation of Ta dimples or Ta oxide nanotubes by anodization. *Nano Lett.* **2006**, *6*, 2995–2999. [[CrossRef](#)]
41. El-Sayed, H.; Singh, S.; Kruse, P. Formation of Dimpled Tantalum Surfaces from Electropolishing. *J. Electrochem. Soc.* **2007**, *154*, C728. [[CrossRef](#)]
42. El-Sayed, H.A.; Birss, V.I. Controlled interconversion of nanoarray of Ta dimples and high aspect ratio Ta oxide nanotubes. *Nano Lett.* **2009**, *9*, 1350–1355. [[CrossRef](#)]
43. Min, X.; Bai, P.; Emura, S.; Ji, X.; Cheng, C.; Jiang, B.; Tsuchiya, K. Effect of oxygen content on deformation mode and corrosion behavior in β-type Ti–Mo alloy. *Mater. Sci. Eng. A* **2017**, *684*, 534–541. [[CrossRef](#)]
44. Fomby, P.; Cherlin, A.J.; Hadjizadeh, A.; Doillon, C.J.; Sueblinvong, V.; Weiss, D.J.; Bates, J.H.T.; Gilbert, T.; Liles, W.C.; Lutzko, C.; et al. Anodic oxide nanotube layers on Ti–Ta alloys: Substrate composition, microstructure and self-organization on two-size scales. *Corros. Sci.* **2006**, *12*, 181–204. [[CrossRef](#)]
45. Tsuchiya, H.; Akaki, T.; Nakata, J.; Terada, D.; Tsuji, N.; Koizumi, Y.; Minamino, Y.; Schmuki, P.; Fujimoto, S. Anodic oxide nanotube layers on Ti–Ta alloys: Substrate composition, microstructure and self-organization on two-size scales. *Corros. Sci.* **2009**, *51*, 1528–1533. [[CrossRef](#)]
46. Porter, J.R.; Henson, A.; Ryan, S.; Popat, K.C. Biocompatibility and Mesenchymal Stem Cell Response to Poly (ε-Caprolactone) Nanowire Surfaces for Orthopedic Tissue Engineering. *Tissue Eng. Part A* **2009**, *15*, 2547–2559. [[CrossRef](#)] [[PubMed](#)]

47. Mat-Baharin, N.H.; Razali, M.; Mohd-Said, S.; Syarif, J.; Muchtar, A. Influence of alloying elements on cellular response and in-vitro corrosion behavior of titanium-molybdenum-chromium alloys for implant materials. *J. Prosthodont. Res.* **2020**. [[CrossRef](#)]
48. Geetha, M.; Singh, A.K.; Asokamani, R.; Gogia, A.K. Ti based biomaterials, the ultimate choice for orthopaedic implants—A review. *Prog. Mater. Sci.* **2009**, *54*, 397–425. [[CrossRef](#)]
49. Mitri, F.F.; Ingle, A.P. The Bone Biology and the Nanotechnology for Bone Engineering and Bone Diseases. In *Nanotechnology in Skin, Soft Tissue, and Bone Infections*; Springer International Publishing: Amravati, India, 2020; pp. 223–244.
50. Lorenzetti, M.; Kulkarni, C.V.; Igljč, A.; Patil-Sen, Y.; Junkar, I.; Kulkarni, M. Wettability studies of topologically distinct titanium surfaces. *Colloids Surf. B* **2015**, *129*, 47–53. [[CrossRef](#)]
51. Capellato, P.; Claro, A.P.R.A.; Silva, G.; Zavaglia, C.A.C. Antimicrobial effect of TiO₂ nanotubes coating for dental implant. *Dent. Mater.* **2018**, *34*, e21. [[CrossRef](#)]
52. Fan, H.; Guo, Z. Bioinspired surfaces with wettability: Biomolecule adhesion behaviors. *Biomater. Sci.* **2020**, *8*, 1502–1535. [[CrossRef](#)]
53. Popa, A.M.; Giazson, M.; Davidson, P.; Ploux, L.; Liley, M.; Anselme, K. The interaction of cells and bacteria with surfaces structured at the nanometre scale. *Acta Biomater.* **2010**, *6*, 3824–3846. [[CrossRef](#)]
54. Capellato, P.; Sachs, D.; Claro, A.P.R.A.; Silva, G.; Zavaglia, C.A.C. Comparative research of bacteria gram-negative and positive on ti-30ta alloy. *Dent. Mater.* **2019**, *35*, e6–e7. [[CrossRef](#)]



© 2020 by the authors. Licensee MDPI, Basel, Switzerland. This article is an open access article distributed under the terms and conditions of the Creative Commons Attribution (CC BY) license (<http://creativecommons.org/licenses/by/4.0/>).